

# Universal interaction-driven gap in metallic carbon nanotubes

Mitchell J. Senger<sup>1</sup>, Daniel R. McCulley<sup>1</sup>, Neda Lotfizadeh<sup>2</sup>, Vikram V. Deshpande<sup>2</sup>, Ethan D. Minot<sup>1\*</sup>

<sup>1</sup>*Department of Physics, Oregon State University, Corvallis, Oregon 97331, USA*

<sup>2</sup>*Department of Physics and Astronomy, University of Utah, Salt Lake City, Utah 84112, USA*

*\*Corresponding Author: [ethan.minot@oregonstate.edu](mailto:ethan.minot@oregonstate.edu)*

## ABSTRACT

Suspended metallic carbon nanotubes (m-CNTs) exhibit a remarkably large transport gap that can exceed 100 meV. Both experiment and theory suggest that strong electron-electron interactions play a crucial role in generating this electronic structure. To further understand this strongly-interacting system, we have performed electronic measurements of suspended m-CNTs with known diameter and chiral angle. Spectrally-resolved photocurrent microscopy was used to determine m-CNT structure. The room-temperature electrical characteristics of 18 individual-contacted m-CNTs were compared to their respective diameter and chiral angle. At the charge neutrality point, we observe a peak in m-CNT resistance that scales exponentially with inverse diameter. Using a thermally-activated transport model, we estimate that the transport gap is  $450 \text{ meV}\cdot\text{nm}/D$  where  $D$  is CNT diameter. We find no correlation between the gap and the CNT chiral angle. Our results add important new constraints to theories attempting to describe the electronic structure of m-CNTs.

## I. INTRODUCTION

Metallic carbon nanotubes (m-CNTs) are an ideal system for exploring one-dimensional (1-d) quantum phases that emerge due to strong electron-electron interactions.<sup>1</sup> Transport

measurements,<sup>2-4</sup> photoemission spectroscopy measurements,<sup>5</sup> and plasmonics measurements<sup>6</sup> have revealed properties consistent with Tomonaga-Luttinger liquid theory.<sup>7-9</sup> Additional transport measurements<sup>10</sup> have been interpreted with Mott insulator theory.<sup>7,9,11-14</sup> Nuclear magnetic resonance measurements<sup>15</sup> have been interpreted with Luther-Emery liquid theory.<sup>16</sup> Additional predictions for interaction-driven phenomena in m-CNTs include charge/spin density waves,<sup>9,11</sup> and an excitonic insulator state.<sup>17</sup> It is clear that strong interactions can generate fascinating electronic phenomena in m-CNTs and it is an ongoing experimental challenge to discover and explore such phenomena.

Scanning tunneling spectroscopy measurements of m-CNTs on gold substrates first showed the existence of a small gap in 2001.<sup>18</sup> On the gold surface (high dielectric screening) the gap scaled inversely with diameter squared, and was interpreted using non-interacting electron theory.<sup>19</sup> Interestingly, transport studies performed during in the same time period did not reveal a similar gap, presumably due to issues with device cleanliness and electrostatic/structural disorder.<sup>20</sup> As the fabrication of CNT devices improved, the energy gap in m-CNTs became observable in transport experiments.<sup>21</sup> A pioneering experiment in 2009 quantified the transport gap in 15 individually-contacted suspended m-CNTs.<sup>10</sup> By utilizing suspended CNTs, Coulomb interactions between charge carriers were unscreened and the interaction-driven effects were enhanced. The experiment revealed gaps that were much larger than the gaps measured by scanning tunneling spectroscopy. Moreover, the gaps could not be closed by axial magnetic field. This 2009 experiment clearly demonstrated the failure of non-interacting-electron theories to describe the energy gap in the electronic structure of m-CNTs.

Theoretical models describing the transport gap of m-CNTs include enhancement of a bare band gap,<sup>22</sup> the opening of a Mott gap,<sup>7,9,11-14</sup> and the opening of an excitonic insulator gap.<sup>17</sup> These theories make a variety of predictions regarding the diameter and chiral angle dependence of the gap. However, comparison between theory and experiment has been limited by insufficient experimental information about the diameter,  $D$ , and chiral angle,  $\theta$ , of the m-CNT under test. For exmple, in reference 10,<sup>10</sup>  $D$  was determined indirectly via the magnetic field dependence of the transport gap, assuming a non-interacting (semiclassical) theory. Later experiments have challenged the validity of this semiclassical relationship between  $D$  and orbital magnetic moment.<sup>23</sup> Similiarly, most electronic measurements of m-CNTs are made without

knowledge of  $\theta$ . For example, in reference 10,<sup>10</sup> the Rayleigh scattering technique<sup>24</sup> was used to identify  $\theta$  of only two m-CNTs.

Experimental progress requires electrically-contacted m-CNTs with precisely characterized  $D$  and  $\theta$ . Such characterization can be achieved using optical techniques, since the absorption spectrum of a particular CNT is uniquely determined by  $D$  and  $\theta$ . Optical absorption resonances have been catalogued for all CNTs up to  $D = 4.75$  nm.<sup>25</sup> Two approaches have emerged to measure CNT optical absorption resonances of individual CNTs: Rayleigh scattering,<sup>24</sup> (Reference 24 should be Sfeir et al. Science 306, 1540 (2004)) and photocurrent spectroscopy.<sup>26,27</sup> Photocurrent spectroscopy has the advantage of working with electrically-contacted CNT devices fabricated on non-transparent substrates. Previous experimenters have applied photocurrent spectroscopy to identify  $D$  and  $\theta$  of semiconducting CNTs (s-CNTs), and here we extend the technique to characterize m-CNTs.

Combining optical characterization with electrical transport measurements, we investigate the electronic structure of m-CNTs. We find a diameter-dependent gap that is larger than previous estimates. The size of the gap scales as  $1/D$ , and shows no correlation to  $\theta$ . We compare our results to existing theories for interaction-driven gaps in m-CNTs.

## II. METHODS

Suspended m-CNT FET devices were grown by chemical vapor deposition to bridge the gap over 2- $\mu$ m-wide trenches. Details of the CVD processing parameters are given in previously published work.<sup>28</sup> The bottom of the trench is 760 nm below the top of the Pt source/drain electrodes (Fig 1). A pair of gate electrodes are located at the bottom of the trench. The gate electrodes are separated by a 250 nm gap. The split-gate geometry allows for homogenous doping of the entire device ( $V_{g1} = V_{g2}$ ) or the generation of a pn junction by doping one half of the device with holes and the other with electrons ( $V_{g1} = -V_{g2}$ ).

After device fabrication is completed, the chiral index of the individual m-CNTs is determined by photocurrent spectroscopy. While previous experiments have demonstrated that photocurrent spectroscopy is capable of measuring chiral index ( $n, m$ ) of s-CNTs,<sup>26,27</sup> this is the

first time that photocurrent spectroscopy has been applied to the chiral identification of m-CNTs. The device is placed in a room-temperature vacuum environment with optical access (Janis cryostat). Spectrally-tunable scanning photocurrent microscopy (SPCM) is used to determine the optical resonance spectra (see Fig. 1). A pn junction is established by setting  $V_{G1} = -V_{G2} = 7$  V or 10 V and  $V_{SD} = 0$ . Photocurrent is generated by illuminating the device with a spectrally-tunable light source (Fianium SC-4 filtered by a double monochromator). The dominant mechanism of photocurrent generation is photovoltaic for CNTs with larger gaps ( $\gtrsim 100$  meV) and photothermoelectric for CNTs with smaller gaps ( $\lesssim 100$  meV).<sup>29,30</sup> Polarization of the linearly polarized light is aligned to CNT axis such that the absorption cross section is maximized.<sup>31</sup> The optical intensity is  $\sim 25$  W/cm<sup>2</sup>. The measured photocurrent spectra are normalized to account for the spectral dependence of the incident photon flux. The photocurrent normalization procedure also accounts for the constructive/destructive interference caused by light reflected from the gate electrodes beneath the CNT.<sup>32</sup> The SPCM image, combined with the photocurrent spectra confirms that a single m-CNT is electrically connected.

The measured photocurrent spectra are compared to an empirical model for the absorption cross-section of suspended CNTs (see Figure 1b).<sup>25,31</sup> Spectral features distinguishing m-CNTs from s-CNTs include wide regions of the spectrum with no resonances, and peak doublets when the chiral angle  $\theta < 30^\circ$ . For all m-CNTs in this study we find a close fit between the normalized photocurrent spectrum and the expected absorption cross-section of a particular m-CNT chiral index.

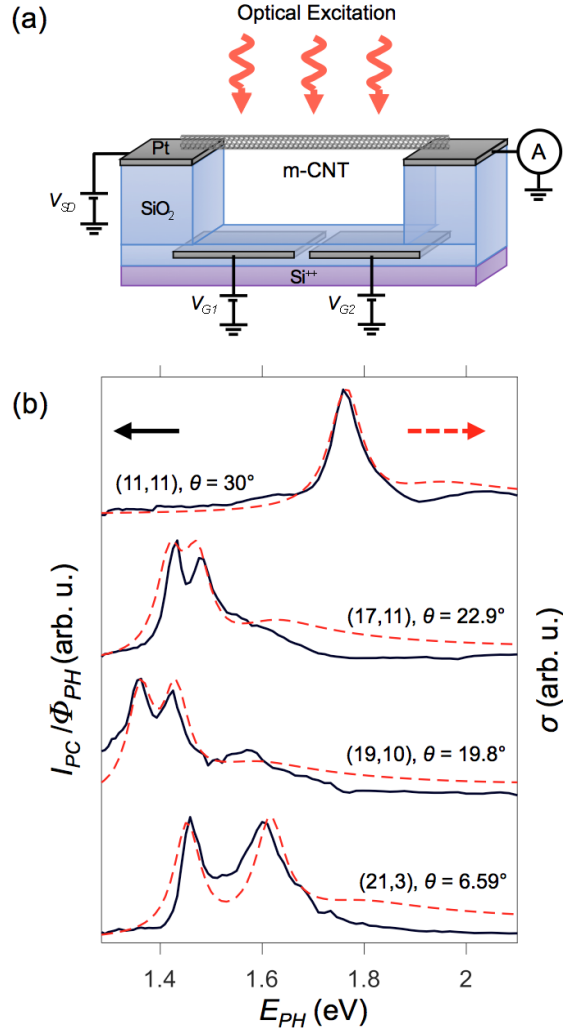


**Figure 1.** Identifying the chiral index of individually-contacted m-CNTs. (a) Schematic diagram showing the split-gate device geometry. (b) The normalized photocurrent spectra (black lines) are compared to the empirical prediction for the optical absorption cross-section (red dash lines). The curves have been vertically offset for clarity.

### III. RESULTS

Figure 2a-c shows the room-temperature  $R(V_g)$  curves from three chirally-identified CNTs. Both gates are set to the same potential, such that  $V_{G1} = V_{G2} = V_g$ . The CNT is p-doped for  $V_g < 1$  V and n-doped for  $V_g > 1$  V. Half-filling of the  $2p_z$  orbitals occurs at approximately  $V_g = 1$  V, corresponding to a peak in CNT resistance. We quantify the resistance peak by calculating  $\Delta R$

$= R_{\text{peak}} - R_c$ , where  $R_c$  is the contact resistance associated with the CNT/Pt interfaces. The fitting procedure for  $R_c$  is described in the SI.<sup>33</sup> Figure 2a-c show the atomic structure of each CNT device under test and the corresponding electrical characteristics. There is a clear trend between  $\Delta R$  and m-CNT diameter (Figure 2d). This trend is explored further below.

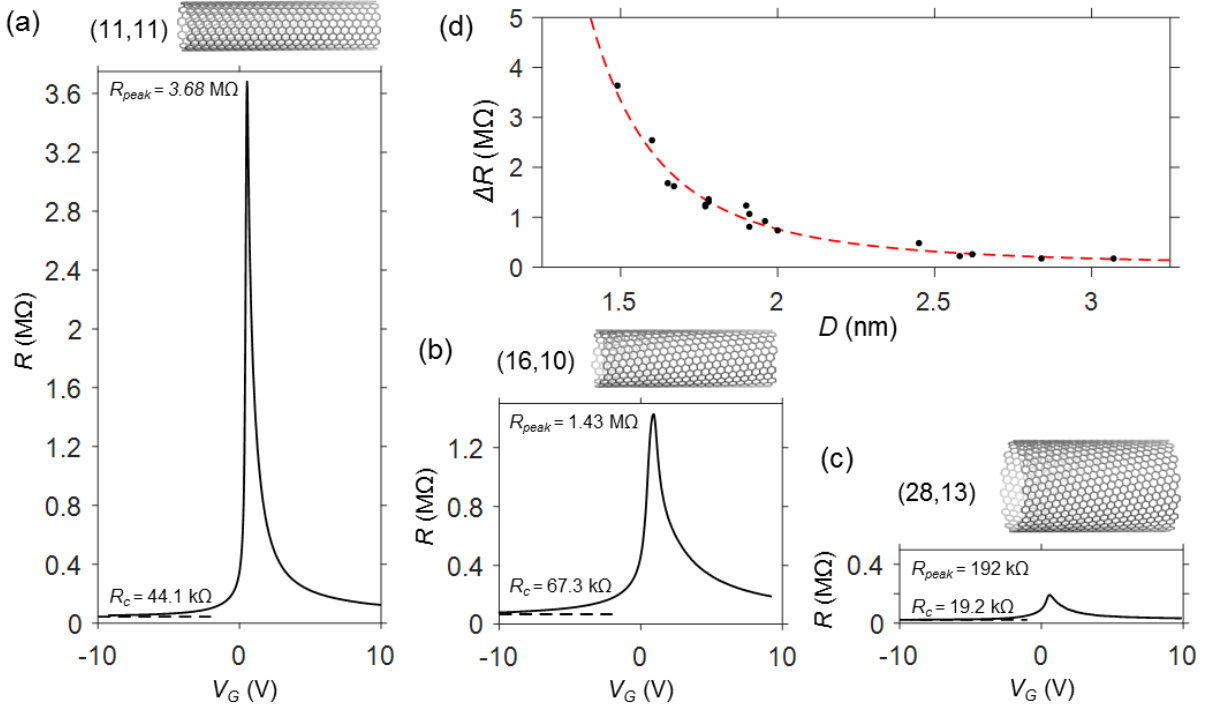


**Figure 2.** Resistance of m-CNTs that have different chiral index. a-c) Peak resistance becomes remarkably large for small diameter m-CNTs. d)  $\Delta R$  plotted against m-CNT diameter.

A total of 18 chirally-identified m-CNTs have been electrically characterized. We find that  $\Delta R$  increases exponentially with inverse diameter. In Figure 3, the measured data is fit to the relationship

$$\Delta R = R_0 \exp(\alpha/D) \quad (1)$$

where  $\alpha = 8.9 \pm 0.2$  nm and  $R_0 = 9.0 \pm 1.0$  k $\Omega$ .

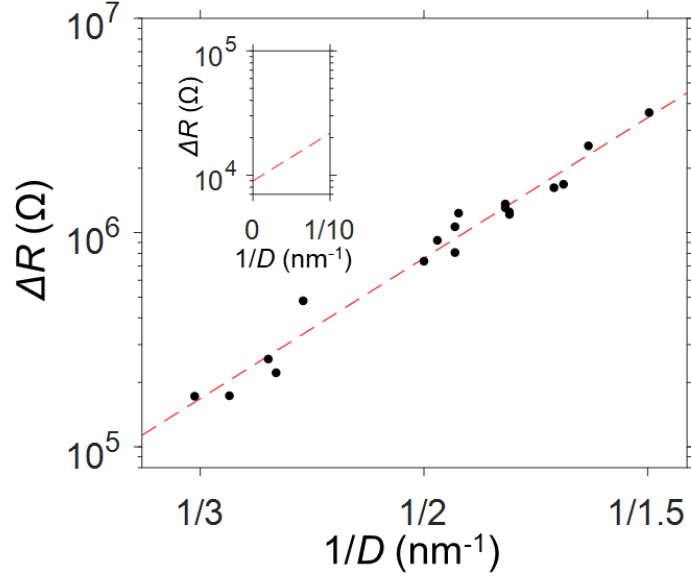


**Figure 3.** Relationship between  $\Delta R$  and inverse diameter for 18 different chirally-identified m-CNTs. The line of best fit (red dashed line) intercepts the y-axis at  $9 \pm 1.0 \text{ k}\Omega$  (inset).

The measured  $\Delta R$  values (Fig. 3) can be interpreted using a thermally-activated transport model. At the charge neutrality point (half filling of the  $2p_z$  orbitals), we assume that free carriers are generated by thermal activation across an energy gap,  $\Delta$ , such that

$$\Delta R = R_0 \exp(\beta\Delta), \quad (2)$$

where  $\beta$  could be  $1/kT$  (activation is across the full energy gap), or  $1/2kT$  (activation across half the energy gap) or something in between. Further discussion of this model, and interpretation of  $R_0$ , are presented in the SI.<sup>33</sup> Equating  $\beta\Delta$  with the exponent in Eq. 1, we estimate a lower and upper bound for the diameter-dependent energy gap,

$$\text{Lower bound: } \Delta = kT\alpha/D = [225 \text{ meV}\cdot\text{nm}]/D \quad (3a)$$

$$\text{Upper bound: } \Delta = 2kT\alpha/D = [450 \text{ meV}\cdot\text{nm}]/D \quad (3b)$$

Previous work by Aspitarte et al. compared room temperature  $R(V_g)$  relationships to Coulomb blockade spectroscopy and determined  $\beta \approx 1/2kT$ .<sup>22</sup> Therefore, we consider Eq. 3b a reasonable estimate of the transport gap.

After establishing the diameter dependence of the gap ( $\Delta \sim 1/D$ ) we consider whether small deviations from the  $1/D$  relationship could be attributed to chiral angle  $\theta$ . If diameter is the only variable affecting  $\Delta R$ , then the experimentally measured parameter  $D \cdot \ln(\Delta R/R_0)$  would be equal to a universal constant. Figure 4 shows  $D \cdot \ln(\Delta R/R_0)$  plotted as function of  $\theta$  for the 18 CNTs in our study. The average value is 8.9 nm and the standard deviation is 0.3 nm. There is no correlation between  $D \cdot \ln(\Delta R/R_0)$  and chiral angle  $\theta$ .

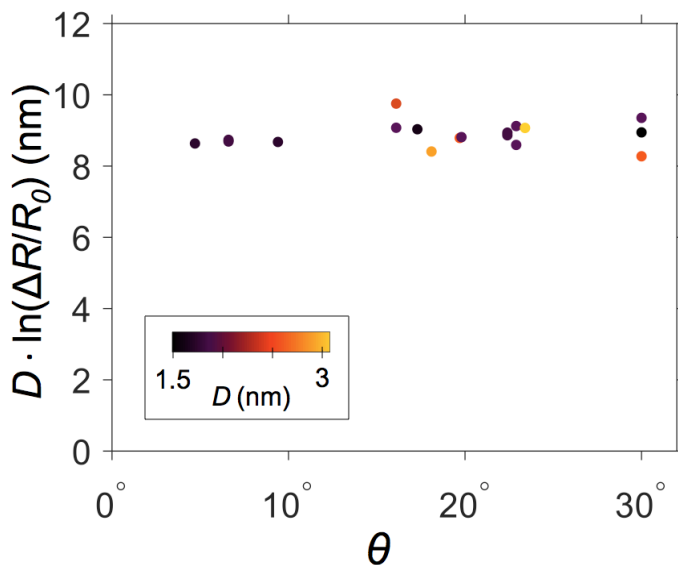


**Figure 4.**  $D \cdot \ln(\Delta R/R_0)$  plotted against  $\theta$  for the 18 m-CNTs in our study. The data points are color coded to indicate CNT diameter.

#### IV. DISCUSSION

From a practical viewpoint, we note that a simple room-temperature measurement of  $\Delta R$  is a remarkably good measurement of diameter for suspended m-CNTs. The data points in Figure 2d fall within 0.1 nm of the fit line. This diameter measurement technique will be useful for experimenters studying suspended m-CNTs.

While our experiments have focused on suspended m-CNTs, we expect that similar transport gaps can be observed in m-CNTs on high-quality insulators such as exfoliated boron nitride.<sup>6</sup> Assuming that the interaction between the substrate and the CNT does not introduce disorder, the main difference between suspended and substrate-bound m-CNTs is dielectric screening. A previous study of suspended m-CNTs in dielectric liquids showed that the gap is modulated by dielectric environment.<sup>22</sup>

As noted in a number of previous experimental studies, m-CNTs with gaps of order 100 meV cannot be explained by non-interacting-electron band theory.<sup>10,22,34,35</sup> Non-interacting theories predict that m-CNTs have a small band gap due to curvature, axial strain, or twist. For example, if curvature is the only perturbation, non-interacting theory predicts a bare band gap<sup>19</sup>

$$E_{g,\text{bare}} \approx \frac{[50 \text{ meV} \cdot \text{nm}^2] \times \cos(3\theta)}{D^2}. \quad (4)$$

For the range of  $D$  studied here, Eq. 4 predicts  $E_{g,\text{bare}} < 20$  meV. Besides the small perturbation due to curvature (Eq. 4), other built-in strains (stretch, twist, bend) are also gap-inducing.<sup>36</sup> Possible evidence for such strain can be seen in optical characterization: the optical absorption resonances of our m-CNTs vary slightly ( $\sim \pm 10$  meV) from the average values published in the CNT Atlas.<sup>25</sup> Such perturbations would account for  $E_{g,\text{bare}} \sim 10$  meV. Lastly, the Peierls transition has been considered as a gap-inducing mechanism in m-CNTs.<sup>37-39</sup> However, due to the stiffness of the carbon-carbon bonds, the estimated gap due to the Peierls transition is  $\sim [2 \text{ meV} \cdot \text{nm}^3]/D^3$ .<sup>39</sup>

A number of theoretical approaches have been used to predict the effect of e-e interactions on the electronic structure of m-CNTs. Perhaps the simplest approach is a Hartree-Fock self-consistent field calculation which predicts an interaction-driven enhancement of any bare band gap.<sup>40</sup> This approach was recently applied to the curvature-induced gap (Eq. 4), predicting an approximately 3-fold enhancement.<sup>22</sup> However, the enhancement factor is still too small to explain the measured values of  $\Delta R$ . Additional gap-opening mechanisms must be at work. When seeking these mechanisms, we must consider the scaling relationship between gap and diameter, and consider previous experimental evidence that the gap does not close when axial magnetic field is applied to the CNT.<sup>10</sup>

There are at least two interaction-driven mechanisms that can account for a non-closing gap in m-CNTs. In early work, Balents et al.,<sup>9</sup> and Krotov et al.<sup>11</sup> argued that short-range (Hubbard-like) interactions open a Mott gap in armchair CNTs ( $\theta = 30^\circ$ ). To extend these models, the effect of long-range Coulomb interactions have also been considered,<sup>7,12-14</sup> yielding a variety of calculations that predict a Mott-like gap in armchair CNTs. Going beyond armchair CNTs, Odintsov et al. showed that their effective Hamiltonian for interacting electrons in the m-CNT has very weak dependence on  $\theta$ , so their theory has a universal applicability to m-CNTs.<sup>12</sup> However, we note that Odintsov et al. do not consider whether band gaps generated by curvature, or strain could break the universality of their results. Pioneering experiments on suspended CNTs<sup>10</sup> were interpreted using the theory of Odintsov et al.,<sup>12</sup> which predicts a Mott gap scaling of  $1/D^{1/(1-g)}$  where  $g$  is the Luttinger parameter (approximately 0.25 for suspended CNTs).

An alternative mechanism that can account for a non-closing gap in m-CNTs is the spontaneous formation of excitons. Recent first principles calculations have established that an armchair CNT can support this excitonic insulator state at charge neutrality.<sup>17</sup> Varsano et al. argue that the excitonic insulator gap scales as  $1/D$ , and is much more sensitive to dielectric environment than the Mott gap.

The first experiment investigating the diameter-dependent gap in suspended m-CNTs found  $\Delta \sim D^{-1.3}$ .<sup>10</sup> Deshpande et al. measured  $D$  indirectly by determining the orbital magnetic moment of electrons in the CNT. There is significant uncertainty in this approach because the semiclassical relationship between  $D$  and orbital magnetic moment could be strongly modified by e-e interactions.<sup>23</sup> In our current work, we have eliminated this source of uncertainty by using photocurrent spectroscopy to directly measure  $D$  and  $\theta$ .

Our experiments provide two key insights that constrain theories attempting to describe the electronic structure of m-CNT. First, we have measured a scaling relationship  $\Delta \sim D^\gamma$ , where  $\gamma = -1.01 \pm 0.04$ . This exponent is significantly different from the previous reported value  $\gamma = -1.3 \pm 0.15$ .<sup>10</sup> As noted above, the difference with respect to previous results may be due to improved determination of  $D$ . Second, our experiments show that  $\Delta$  is uncorrelated to  $\theta$ . If we assume  $\Delta \propto \ln(\Delta R/R_0)$ , then our experiments show that  $D \cdot \Delta$  is a universal constant within a standard deviation of 4% (Fig. 4). This result supports the concept of a universal gap that is dominated by

diameter-dependent interaction effects, rather than other structural features such as chirality or mechanical strain.

Our analysis (Eq. 3b) suggests that the m-CNTs measured here have gaps ranging from 150 – 300 meV, significantly larger than the gaps measured by Deshpande et al. (20 – 100 meV).<sup>10</sup> The origin of this difference is unknown, however, we speculate that device geometry may play a role. The suspended CNTs in our experiments are strung over a 10-fold longer distance and are higher above the metal gates. This difference in geometry affects the length scale of the long-range Coulomb interaction. Future experiments exploring a variety of device geometries is needed to test this hypothesis.

The magnitude of the gap reported here (Eq 3a,b) is similar to the exciton binding energy in s-CNTs. Dukovic et al. studied exciton binding in s-CNTs of known chiral index and found  $E_b = [340 \text{ meV}\cdot\text{nm}]/D$ . Dukovic et al. also showed that  $E_b$  is independent of  $\theta$ .<sup>41</sup> It is intriguing that  $\Delta$  in our long, suspended m-CNTs is so similar to  $E_b$  in s-CNTs. While it may be a coincidence, we note that both energies,  $\Delta$  and  $E_b$ , coincide with the characteristic energy scale for Coulomb interaction in CNTs,  $e^2/4\pi\epsilon D$ .

## V. CONCLUSION

In conclusion, we have measured the structural dependence of the energy gap,  $\Delta$ , in suspended m-CNTs. In contrast to previous reports, we find that the energy gap scales as  $1/D$ . Our measurements show that  $D\cdot\Delta$  is a universal constant to within 4% standard deviation. A key observation is that  $D\cdot\Delta$  is insensitive to chiral angle. The magnitude of  $\Delta$  is significantly larger than previous measurements, perhaps due to the greater length scale for the unscreened Coulomb interactions. These results add important new constraints on theories attempting to describe exotic electronic structure of m-CNTs.

## ACKNOWLEDGMENTS

We thank Massimo Rontani for valuable discussions. This material is based upon work supported by the National Science Foundation under Grant No. 1709800. A portion of device fabrication was carried out in the University of California Santa Barbara (UCSB) nanofabrication facility.

- 
- 1 V. V Deshpande, M. Bockrath, L. I. Glazman, and A. Yacoby, *Nature* **464**, 209 (2010).
- 2 Y. Zhen, H. W. C. Postma, L. Balents, and C. Dekker, *Nature* **402**, 273 (1999).
- 3 B. Gao, A. Komnik, R. Egger, D. C. Glatli, and A. Bachtold, *Phys. Rev. Lett.* **92**,  
216804-1 (2004).
- 4 M. Bockrath, D. H. Cobden, A. G. Rinzler, R. E. Smalley, L. Balents, and P. L. McEuen,  
*Nature* **397**, 598 (1999).
- 5 H. Ishii, H. Kataura, H. Shiozawa, H. Yoshioka, H. Otsubo, Y. Takayama, T. Miyahara, S.  
Suzuki, Y. Achiba, M. Nakatake, T. Narimura, M. Higashiguchi, K. Shimada, H.  
Namatame, and M. Taniguchi, *Nature* **426**, 540 (2003).
- 6 Z. Shi, X. Hong, H. A. Bechtel, B. Zeng, M. C. Martin, K. Watanabe, T. Taniguchi, Y.-R.  
Shen, and F. Wang, *Nat. Photonics* **9**, 515 (2015).
- 7 R. Egger and A. O. Gogolin, *Phys. Rev. Lett.* **79**, 5082 (1997).
- 8 C. Kane, L. Balents, and M. P. A. Fisher, *Phys. Rev. Lett.* **79**, 5086 (1997).
- 9 L. Balents and M. P. A. Fisher, *Phys. Rev. B* **55**, R11973 (1997).
- 10 V. V Deshpande, B. Chandra, R. Caldwell, D. S. Novikov, J. Hone, and M. Bockrath,  
*Science* **323**, 106 LP (2009).
- 11 Y. A. Krotov, D. H. Lee, and S. G. Louie, *Phys. Rev. Lett.* **78**, 4245 (1997).
- 12 A. A. Odintsov and H. Yoshioka, *Phys. Rev. B* **59**, R10457 (1999).
- 13 A. A. Nersesyan and A. M. Tsvelik, *Phys. Rev. B* **68**, 235419 (2003).
- 14 H. Yoshioka and A. A. Odintsov, *Phys. Rev. Lett.* **82**, 374 (1999).
- 15 P. M. Singer, P. Wzietek, H. Alloul, F. Simon, and H. Kuzmany, *Phys. Rev. Lett.* **95**,  
236403-1 (2005).

- 16 B. Dóra, M. Gulácsi, F. Simon, and H. Kuzmany, *Phys. Rev. Lett.* **99**, 166402-1 (2007).
- 17 D. Varsano, S. Sorella, D. Sangalli, M. Barborini, S. Corni, E. Molinari, and M. Rontani, *Nat. Commun.* **8**, 1461 (2017).
- 18 M. Ouyang, J. L. Huang, C. L. Cheung, and C. M. Lieber, *Science* **292**, 702 (2001).
- 19 C. L. Kane and E. J. Mele, *Phys. Rev. Lett.* **78**, 1932 (1997).
- 20 E. A. Laird, F. Kuemmeth, G. A. Steele, K. Grove-Rasmussen, J. Nygård, K. Flensberg, and L. P. Kouwenhoven, *Rev. Mod. Phys.* **87**, 703 (2015).
- 21 J. Cao, Q. Wang, and H. Dai, *Nat. Mater.* **4**, 745 (2005).
- 22 L. Aspirtarte, D. R. McCulley, A. Bertoni, J. O. Island, M. Ostermann, M. Rontani, G. A. Steele, and E. D. Minot, *Sci. Rep.* **7**, 8828 (2017).
- 23 G. A. Steele, F. Pei, E. A. Laird, J. M. Jol, H. B. Meerwaldt, and L. P. Kouwenhoven, *Nat. Commun.* **4**, 1573 (2013).
- 24 M. Y. Sfeir, F. Wang, L. Huang, C. C. Chuang, J. Hone, P. O'Brien S, T. F. Heinz, and L. E. Brus, *Science* **306**, 1540 (2004).
- 25 K. Liu, J. Deslippe, F. Xiao, R. B. Capaz, X. Hong, S. Aloni, A. Zettl, W. Wang, X. Bai, S. G. Louie, E. Wang, and F. Wang, *Nat. Nanotechnol.* **7**, 325 (2012).
- 26 A. Malapanis, V. Perebeinos, D. P. Sinha, E. Comfort, and J. U. Lee, *Nano Lett.* **13**, 3531 (2013).
- 27 T. Deborde, L. Aspirtarte, T. Sharf, J. W. Kevek, and E. D. Minot, *J. Phys. Chem. C* **118**, 9946 (2014).
- 28 T. Sharf, J. W. Kevek, and E. D. Minot, in *2011 11th IEEE Int. Conf. Nanotechnol.* (IEEE, 2011), pp. 122–125.
- 29 M. R. Amer, S. W. Chang, and S. B. Cronin, *Small* **11**, 3119 (2015).
- 30 G. Buchs, S. Bagiante, and G. A. Steele, *Nat. Commun.* **5**, 4987 (2014).

- 31 K. Liu, X. Hong, S. Choi, C. Jin, R. B. Capaz, J. Kim, W. Wang, X. Bai, S. G. Louie, E.  
Wang, and F. Wang, Proc. Natl. Acad. Sci. **111**, 7564 (2014).
- 32 L. Aspirtarte, D. R. McCulley, and E. D. Minot, Nano Lett. **16**, 5589 (2016).
- 33 See Supplemental Material at [URL] for an analysis of  $\Delta R$  using the Landauer transport  
model, and a description of the method used to determine  $R_c$ .
- 34 M. R. Amer, A. Bushmaker, and S. B. Cronin, Nano Lett. **12**, 4843 (2012).
- 35 S. W. Chang, R. Dhall, M. Amer, K. Sato, R. Saito, and S. Cronin, Nano Res. **6**, 736  
(2013).
- 36 L. Yang and J. Han, Phys. Rev. Lett. **85**, 154 (2000).
- 37 K.-P. Bohnen, R. Heid, H. J. Liu, and C. T. Chan, Phys. Rev. Lett. **93**, 245501-1 (2004).
- 38 D. Connétable, G.-M. Rignanese, J.-C. Charlier, and X. Blase, Phys. Rev. Lett. **94**,  
015503-1 (2005).
- 39 W. Chen, A. V. Andreev, A. M. Tselik, and D. Orgad, Phys. Rev. Lett. **101**, 246802-1  
(2008).
- 40 T. Ando, J. Phys. Soc. Japan **74**, 777 (2005).
- 41 G. Dukovic, F. Wang, D. Song, M. Y. Sfeir, T. F. Heinz, and L. E. Brus, Nano Lett. **5**,  
2314 (2005).